Extended Data:

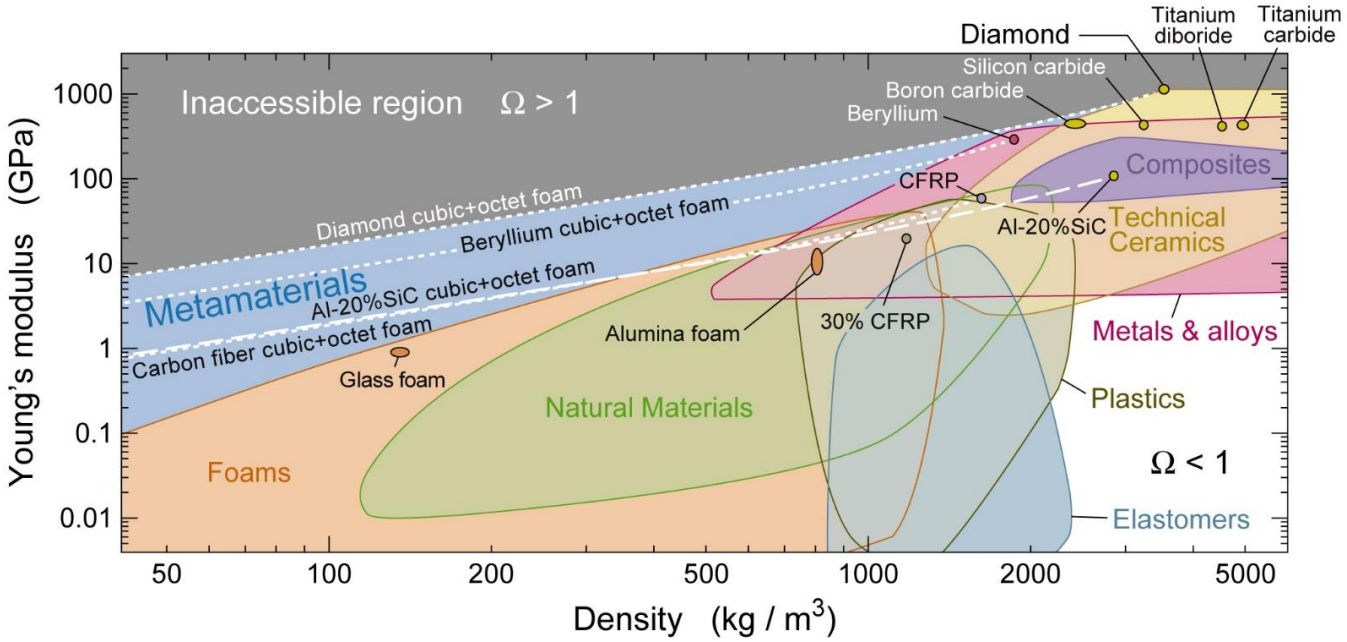

Extended Data Figure 1 | Property space of isotropic and nearly isotropic materials. Metamaterial geometries with suboptimal performance have been omitted. Theoretical bounds, $\Omega = 1$, limits the performance of all material systems and is defined by the highest performance possible for a two-phase system, achieved by the single crystal diamond and void system. The parameter Ω is defined in the text. The cubic+octet material can pragmatically bound property space when composed of materials with maximal properties, such as diamond, beryllium, fiber composites, and lightweight alloys. Fabrication techniques now limit our ability to achieve a wide and otherwise unoccupied region of property space.

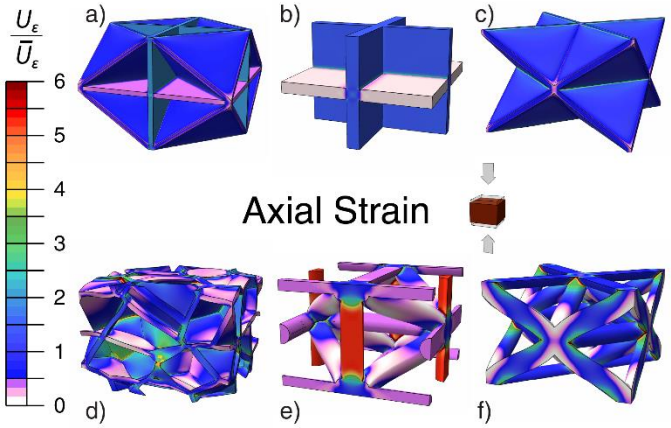

Extended Data Figure 2 | Strain energy distributions from axial stress. Strain energy distributions in the geometries from FIG.1 subject to uniaxial stress; where U_ε is the local strain energy density, and $\bar{U}_\varepsilon$ is the average solid phase strain energy density. Macroscopic loads are transmitted through stiff networks of members aligned with the principal stress direction. Strains are small but scaled to reveal the nature of the deformations. The two-dimensional connectedness of material in closed cell geometries allows for the effective transmission of loads between neighboring members, facilitating materials that can achieve the theoretical bounds (a). Open cell and stochastic materials (bottom row) have significant strain energy concentrations.

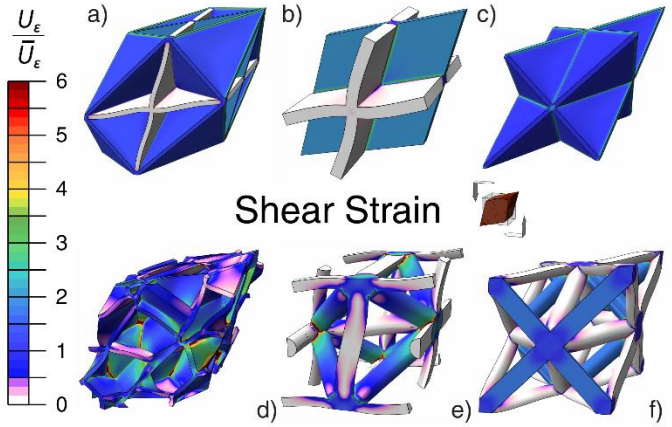

Extended Data Figure 3 | Strain energy distributions from shear loading. Strains are scaled to highlight the nature of the deformations. The displacements in stiff closed cell materials (top row) are largely affine and absent of bending. Despite the identical alignment of material in the OT (f) and OF (c), the absence of membrane stress allows significant bending to take place in the open cell configuration. All geometries have, $(\bar{\rho}/\rho_S) = 0.2$.

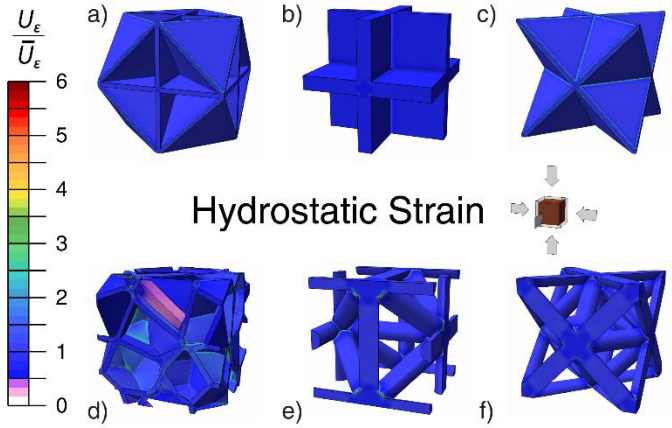

Extended Data Figure 4 | Strain energy distributions from hydrostatic loading. Strains are scaled to highlight the nature of the deformations. In maximally stiff materials, the deformations are limited to the filling of void space through member swelling. The displacements are primarily affine and strain energy distributions nearly uniform. Poor alignment of neighboring cell walls in the QR material allows some bending to occur (d). All geometries have, $(\bar{\rho}/\rho_S) = 0.2$.

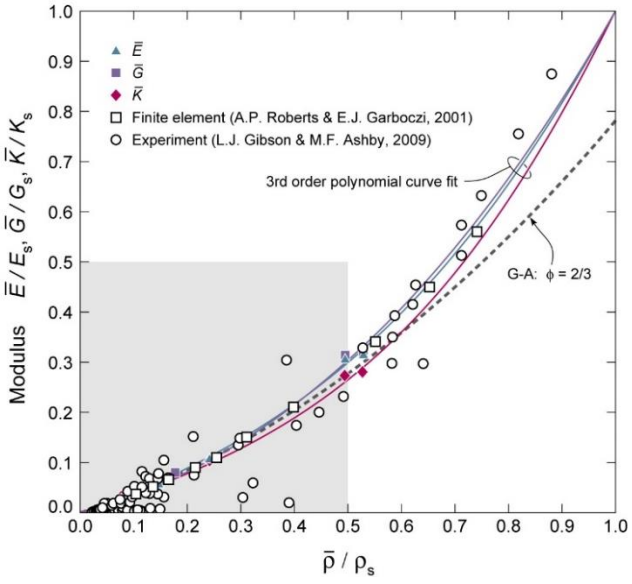

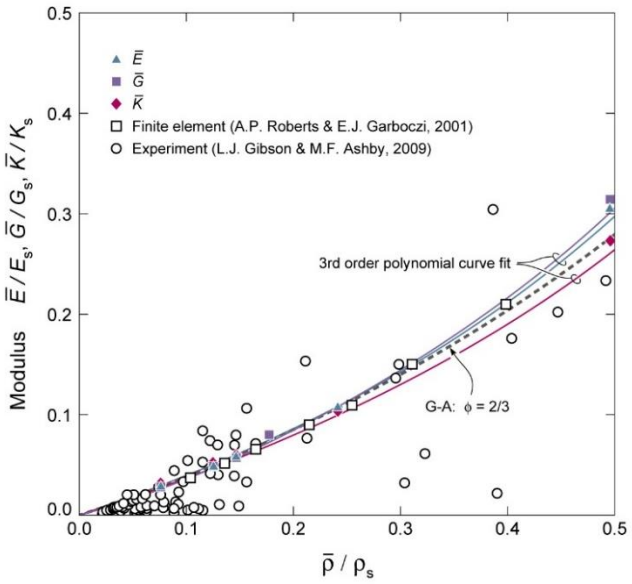

Extended Data Figure 5 | Moduli of Quasi-Random and stochastic foams. The normalized average Young's, shear, and bulk moduli of quasi-random foam finite element (FE) models plotted against relative density. Data are fit to third order polynomials, forced to go through the origin (0, 0) and the point (1, 1), corresponding to empty space and a dense solid respectively. Data are also fit to the Gibson and Ashby model for the stiffness of isotropic cellular materials. Experimental data for Young's modulus are taken from L.J. Gibson and M.F. Ashby[24].

Extended Data Table 1 | Materials properties used to populate property space. Select engineering materials used to populate Young's modulus vs. density space as constituents for metamaterials (FIG.ED1).

Material	Young's Modulus	Density
	(GPa)	(kg/m^3)
Diamond	1180	3250
Beryllium	300	1850
Al-SiC20%	110	2855
CFRP Quasi-isotropic unidirectional laminate (in plane)	55	1550